Neuro-Oncology

25(6), 1031–1043, 2022 | https://doi.org/10.1093/neuonc/noac233 | Advance Access date 10 October 2022

TRIM67 drives tumorigenesis in oligodendrogliomas through Rho GTPase-dependent membrane blebbing

Engin Demirdizen[†], Ruslan Al-Ali[1,†], Ashwin Narayanan[2], Xueyuan Sun, Julianna Patricia Varga[3], Bianca Steffl, Manuela Brom, Damir Krunic, Claudia Schmidt, Gabriele Schmidt, Felix Bestvater, Julian Taranda, and Şevin Turcan

Neurology Clinic and National Center for Tumor Diseases, University Hospital Heidelberg, INF 460, Heidelberg, Germany (E.D., R. A-A., A.N., X.S., P.V., B.S., J.T., Ş.T.) Clinical Cooperation Unit Neurooncology, German Consortium for Translational Cancer Research (DKTK), German Cancer Research Center (DKFZ), Heidelberg, Germany (X.S., B.S.); Core Facility Unit Light Microscopy, German Cancer Research Center (DKFZ), Im Neuenheimer Feld 280, 69120 Heidelberg, Germany (M.B., D.K., C.S., G.S., F.B.,)

[†]Equal contribution.

Corresponding Author: Şevin Turcan, Neurology Clinic and National Center for Tumor Diseases, University Hospital Heidelberg, INF 460, Heidelberg, Germany (sevin.turcan@med.uni-heidelberg.de).

[1]Present address: Centogene GmbH, Am Strande 7, 18055 Rostock, Germany.
[2]Present address: QV Bioelectronics, Manchester, UK.
[3]Present address: EMBO, Meyerhofstraße 1, 69117 Heidelberg, Germany.

Abstract

Background. IDH mutant gliomas are grouped into astrocytomas or oligodendrogliomas depending on the codeletion of chromosome arms 1p and 19q. Although the genomic alterations of IDH mutant gliomas have been well described, transcriptional changes unique to either tumor type have not been fully understood. Here, we identify Tripartite Motif Containing 67 (TRIM67), an E3 ubiquitin ligase with essential roles during neuronal development, as an oncogene distinctly upregulated in oligodendrogliomas.

Methods. We used several cell lines, including patient-derived oligodendroglioma tumorspheres, to knock down or overexpress TRIM67. We coupled high-throughput assays, including RNA sequencing, total lysate-mass spectrometry (MS), and coimmunoprecipitation (co-IP)-MS with functional assays including immunofluorescence (IF) staining, co-IP, and western blotting (WB) to assess the *in vitro* phenotype associated with TRIM67. Patient-derived oligodendroglioma tumorspheres were orthotopically implanted in mice to determine the effect of TRIM67 on tumor growth and survival.

Results. TRIM67 overexpression alters the abundance of cytoskeletal proteins and induces membrane bleb formation. TRIM67-associated blebbing was reverted with the nonmuscle class II myosin inhibitor blebbistatin and selective ROCK inhibitor fasudil. NOGO-A/Rho GTPase/ROCK2 signaling is altered upon TRIM67 ectopic expression, pointing to the underlying mechanism for TRIM67-induced blebbing. Phenotypically, TRIM67 expression resulted in higher cell motility and reduced cell adherence. In orthotopic implantation models of patient-derived oligodendrogliomas, TRIM67 accelerated tumor growth, reduced overall survival, and led to increased vimentin expression at the tumor margin.

Conclusions. Taken together, our results demonstrate that upregulated TRIM67 induces blebbing-based rounded cell morphology through Rho GTPase/ROCK-mediated signaling thereby contributing to glioma pathogenesis.

Key Points

- TRIM67 is overexpressed in oligodendrogliomas.
- TRIM67 triggers membrane blebbing through Rho-mediated signaling.
- TRIM67 upregulation leads to increased tumor burden and reduced survival in mice.

Importance of the Study

We identify *TRIM67* as a novel oncogene in oligodendroglioma that leads to increased cell motility, tumor growth, reduced adhesion, and reduced survival in mice. Our results show constitutive TRIM67 expression transforms cell morphology from an adherent to a rounded appearance with membrane blebs. Mechanistic alteration of the actin cytoskeleton and Rho GTPase signaling upon TRIM67 upregulation underlies the rounded cell structure and the membrane blebbing phenotype. TRIM67-induced blebbing is specifically regulated by NOGO-A/RHOA/RAC1/ROCK2 signaling axis. In orthotopic implantation models of oligodendrogliomas, TRIM67 upregulation leads to increased glioma-specific vimentin expression around the tumor edge and leads to increased tumor volume and poor survival. Consistently TRIM67 knockdown increases overall survival in preclinical oligodendroglioma models. Overall, our study highlights TRIM67 as a novel player orchestrating cytoskeleton, Rho GTPase signaling and bleb-based cell movement, ultimately causing tumorigenic outcomes. Therefore, TRIM67 and its downstream mechanisms may be utilized as potential drug targets to treat oligodendrogliomas.

Lower-grade gliomas (LGGs) harbor recurrent mutations in the isocitrate dehydrogenase (IDH) gene.[1,2] IDH mutant LGGs are classified into 2 subtypes based on the presence (oligodendroglioma) or absence (astrocytoma) of chromosome arms 1p and 19q codeletion. Although the mutational landscape of oligodendrogliomas and astrocytomas has been largely elucidated,[1] subtype-specific nonmutational mechanisms and their impact on glioma growth are not well understood.

In this study, we identify *TRIM67* as a distinctly expressed gene in oligodendrogliomas. TRIM67 is a member of the large family of the tripartite motif (TRIM) containing RING finger E3 ubiquitin ligases.[3] TRIM67 is highly expressed in the cerebellum, interacts with TRIM9 and the netrin receptor DCC, and plays a role in neurodevelopment.[4,5] It antagonizes TRIM9-dependent degradation of VASP and positively regulates filopodia extension and axon branching.[6] TRIM67 and TRIM9 associate with cytoskeletal proteins and synaptic regulators, play a role in exocytosis and endocytosis, and are new targets in paraneoplastic cerebellar degeneration associated with lung adenocarcinoma.[7–9]

TRIM67 plays pivotal roles in various cancers. TRIM67 inhibits Ras signaling and activates differentiation in mouse neuroblastoma cells[10] and suppresses colorectal cancer by activating p53.[11] In nonsmall cell lung cancer (NSCLC), TRIM67 upregulates Notch signaling and causes proliferation, migration, and invasion.[12] Although the role of TRIM67 in neuronal development has been elegantly demonstrated, it is unclear whether TRIM67 has an oncogenic role in gliomas.

Here, we aim to characterize the mechanistic role of TRIM67 in glioma pathogenesis. To investigate this, we used patient-derived glioma tumorspheres with or without IDH mutation and 1p/19q codeletion. Additionally, we used SK-N-BE(2) neuroblastoma cell line with endogenously expressed TRIM67 to further analyze the outcomes of TRIM67 manipulation. We find TRIM67 induces membrane blebbing through Rho GTPase-mediated signaling, leading to reduced adhesion, and increased cell motility and tumor expansion.

Materials and Methods

Complete methods can be found in Supplementary Methods.

Cell Culture

Human neural progenitor cells (hNPCs) and patient-derived glioma lines TS603, SU-AO3, S24, TS600, and TS543 were maintained in NeuroCult Basal Medium with proliferation supplements, 20 ng/ml EGF, 20 ng/ml basic-FGF and 2 μg/ml Heparin (StemCell Technologies). S24 Tdtomato/GFP cells were kindly provided by Dr. Varun Venkataramani (Heidelberg University Hospital) and SU-AO3 cells were kindly provided by Dr. Michelle Monje (Stanford University). HEK293TN and SK-N-BE(2) cell lines were maintained in DMEM containing 10% FBS. Blebbistatin (Merck) treatment (20 μM) was performed for 1 h. Fasudil (HA-1077, Selleckchem) treatment (10 μM) was performed for 16 h.

Cloning of pLVX-puro-TRIM67-Flag Overexpression Plasmid

FLAG-TRIM67 was cloned into pLVX-puro (Addgene) using BamHI and SalI. Insert amplification was performed using

the Kappa Hi-Fi Hotstart ReadyMix (Roche). Ligations were performed using Quick Ligation Kit (NEB) and transformed into 50 μL Stbl3 competent E-coli. The plasmid was extracted using the Maxiprep kit (Qiagen).

Viral transductions

TRIM67 was stably overexpressed by viral transduction using pLVX-puro (Addgene) and pLVX-puro-TRIM67-Flag plasmids. Luciferase expression was stably induced by second viral transduction using pHIV-luc-ZsGreen (Addgene) plasmid and zsGreen expressing cells were sorted by flow cytometry. SK-N-BE(2) and SU-AO3 cells were transduced with TRIM67 Mission lentiviral shRNA plasmids (Sigma). For virus production, HEK293TN cells were transiently transfected with the plasmid of choice with FuGene (Promega) and OptiMem (Gibco). Cells were transfected with packaging plasmid psPAX2 (Addgene), envelope plasmid pCMV-VSV-G (Addgene), and expression plasmid in a 1:1:1 ratio. 0.5 μg/ml puromycin selection was applied.

SDS-page and western blot

Cells were lysed in M-PER buffer (Thermo Fisher Scientific) containing 1× Protease Inhibitor Cocktail (Roche). For GTP pulldown, TS603 cells were seeded in NeuroCult without EGF/bFGF. After 24 h serum starvation, the medium was changed to NeuroCult containing 50 ng/μl EGF. Cells were harvested after 15 min EGF induction and flash frozen in liquid nitrogen. RHOA/RAC1/CDC42 Activation Assay Combo kit (Cytoskeleton) manufacturer's protocol was performed. Primary antibodies: Mouse anti-RAC1 (Cytoskeleton #ARC03, 1:250), mouse anti-RHOA (Cytoskeleton #ARH05, 1:500), rabbit anti-ROCK2 (Cell Signaling #9029, 1:1000), rabbit anti-Tensin-2 (Cell Signaling #11990, 1:1000), rabbit anti-FAK (Cell Signaling #3285, 1:1000), rabbit anti-phospho-FAK (Cell Signaling #8556, 1:1000), mouse anti-Flag (Sigma #F1804, 1:1000), mouse anti-Akt (Cell Signaling #2920, 1:2000), rabbit anti-phospho-Akt (Cell Signaling #4060, 1:2000), rabbit anti-Vimentin (Cell Signaling #3932, 1:1000), rabbit anti-GAPDH (Cell Signaling #2118, 1:1000), rabbit anti-TRIM67 (Novus Bio #NBP1-55028, 1:1000), mouse anti-TRIM9 (Abnova #ABN-H00114088-M01, 1:1000), rabbit anti-GFP (Novus Bio #NB600-308, 1:1000), rabbit anti-NOGO-A (Cell Signaling #13401, 1:1000). Secondary antibodies: HRP-linked anti-mouse IgG (Cell Signaling #7076, 1:5000), HRP-linked anti-rabbit IgG (Cell Signaling #7074, 1:5000).

Orthotopic Transplantation

All mouse experiments were approved by the Institutional Animal Care and Use Committee at DKFZ. Female athymic nude mice (7 weeks old) were intracranially injected using a fixed stereotactic apparatus (Stoelting). Mice were orthotopically implanted as previously described.[13] Using a stereotactic frame, 5000 or 50 000 cells were injected into the cortex at a speed of 1 μL/min. The following coordinates from bregma were used: Anterior–posterior = −1.5 mm; mediolateral = +1.5mm; dorsoventral = −1.5 mm.

Bioluminescence Imaging

Bioluminescence imaging (BLI) was performed following i.p. injection of D-luciferin and measured using the Xenogen IVIS Spectrum *in vivo* imaging system (PerkinElmer). Living Image software (PerkinElmer) was used to acquire and analyze the BLI data.

Immunofluorescence

A total of 50 000 cells/well were seeded in Matrigel-coated 24-well dishes. Cells were fixed with 4% PFA for 20 min at RT, permeabilized using PBS-T for 10 min at RT, and blocked in 5% BSA/PBS-T for 30 min at RT. Primary antibodies: Phalloidin-iFluor 594 conjugated (Abcam #176757, 1:1000), mouse anti-F-actin (NH3) (Abcam #ab205, 1:100), mouse anti-Flag (Sigma #F1804, 1:200), mouse anti-TRIM9 (Abnova #ABN-H00114088-M01, 1:200), rabbit anti-NOGO-A (Cell Signaling #13401, 1:200), rabbit anti-cleaved-CASP3 (Cell Signaling #9664, 1:500), rabbit anti-cleaved-PARP (Cell Signaling #5625, 1:400). Secondary antibodies: Alexa Fluor 488 goat anti-mouse (Thermo Fisher Scientific #A-11029, 1:1000), Alexa Fluor 488 donkey anti-rabbit (Thermo Fisher Scientific #A-21206, 1:1000), Alexa Fluor 594 goat anti-mouse (Thermo Fisher Scientific #A-11032, 1:1000), Alexa Fluor 594 donkey anti-rabbit (Thermo Fisher Scientific #A-21207, 1:1000).

Microscopy Imaging and Quantification

The image z-stacks acquisition of DAPI, Alexa-488, and Alexa-594 signal was performed with a Leica TCS SP5 II Confocal microscope. The 3D z-stack projections were prepared using Fiji.[14] F-Actin intensity quantification was performed using in-house developed Fji macros. Image acquisition for IHC-stained sections were performed using ZEN software on Zeiss Cell Observer Z1 microscope.

Embedding, Microtome Sectioning, Immunohistochemistry, and H&E Staining

For IHC and H&E staining, 5-μm thick FFPE sections were stained with the following antibodies: Rabbit monoclonal anti-Flag (Abcam # ab205606, 1:500), rabbit monoclonal anti-Ki-67 (human) (Abcam # ab16667, 1:100), and mouse monoclonal anti-Vimentin (human) (Santa Cruz, # sc6260, 1:25).

Wound Healing

SK-N-BE(2) and TS600 lines were seeded at 5 × 10^5 cells/well density in 6-well plates. The wound was created using a P100 tip in each well. Images were taken at 24 h and 48 h using Nikon Eclipse Ts2 bright-field microscope at 4× magnification. Wound area was quantified using in-house developed Fiji macros.

Cell adhesion

A total of 48-well ECM cell adhesion assay (Cell Biolabs) was performed according to the manufacturer's protocol.

Briefly, EV and TRIM67 overexpressing (TRIM67^{OE}) TS603 cells were seeded at 5 × 10^4 cells/well density in a 48-well ECM-coated plate and incubated for 2.5 h in EGF/FGF-free medium. After incubation with cell stain solution, washing, and extraction, OD was measured at 560 nm in the Infinite 200 Pro plate reader (Tecan).

RNA Sequencing and Bioinformatic Analysis

EV or TRIM67^{OE} cells were seeded at 5 × 10^5 cells/well density in 6-well plates in triplicates and harvested after 48 h. Total RNA was extracted using the QIAGEN RNeasy RNA isolation kit according to the manufacturer's protocol. Sequencing was performed at the DKFZ genomics and proteomics core facility. Raw count normalization and differential expression analysis were performed using DESeq2 R package[15] and Galaxy.[16] An adjusted *P*-value of 0.05 was used as a cutoff to filter the significantly altered genes. Enriched pathways were determined using the Ingenuity Pathway Analysis or Enrichr.[17] Normalized RNA-seq expression for LGGs were obtained from The Cancer Genome Atlas, and ATAC-seq data were obtained from Corces *et al.*[18]

Immunoprecipitation and Mass Spectrometry

Cell lysates from 5 × 10^6 cells were prepared using the IP buffer (50 mM Tris pH 7.5, 150 mM NaCl, 1% TritonX-100, 0.5% Na-DOC, 1 mM EDTA, 2 mM PMSF and 1 × Roche protease inhibitor cocktail). Flag (Sigma #F1804) antibody (2 μg) were added to CTRL/TRIM67 IP samples. Reaction was incubated for 1h at 4°C on a rotator. 25 μL Protein G agarose beads (Roche) were placed into each IP sample and incubated O/N at 4°C on a rotator. Proteins were eluted using 2 × Laemmli buffer (Bio-Rad) at 95°C for 5 min at 1000 rpm. Proteomics were performed at the Mass Spectrometry (MS) Core Facility at the German Cancer Center (DKFZ).

Statistical Analysis

Two-tailed t-test was performed if not stated otherwise using Prism9. Significance is indicated using the following legend: ≤0. 05 (*), ≤0.01 (**), ≤0.001 (***). Survival analysis was performed using a log-rank test in Prism9.

Accession Numbers

RNA-seq data have been deposited in NCBI's Gene Expression Omnibus under accession number GSE184567.

Results

TRIM67 is Overexpressed in Oligodendrogliomas.

To determine the transcriptional differences between oligodendrogliomas and astrocytomas, we analyzed LGG samples from The Cancer Genome Atlas RNA sequencing (RNA-seq) dataset. We identified *TRIM67* as 1 of the most significantly upregulated genes in oligodendrogliomas (Figure 1A, Supplementary Figure 1A). *TRIM67* expression was increased approximately 3.5-fold in oligodendrogliomas compared to astrocytomas or GBM (Figure 1A). A pan-cancer comparison showed *TRIM67* expression is high in LGGs (i.e., oligodendrogliomas) than in most other tumor types, except for neuroblastoma and paraganglioma (Supplementary Figure 1B, C). In the adult human brain, *TRIM67* expression seems to be particularly enriched in medial ganglionic eminence-derived interneurons (Supplementary Figure 1D). *TRIM67* upregulation in oligodendrogliomas may be due to an epigenetic control mechanism involving promoter hypomethylation[19] and open chromatin structure (Supplementary Figure 1E, F). Overall, these results suggest TRIM67 may play a role in oligodendroglioma pathogenesis.

TRIM67 Alters Pathways Regulating Cytoskeletal Organization

To uncover the role of TRIM67 in gliomas, we used 2 patient-derived oligodendroglioma lines (TS603 and SU-AO3), 3 patient-derived GBM lines (S24, TS600, and TS543), and cultured hNPCs (Supplementary Figure 2A). Of the 2 oligodendroglioma lines, SU-AO3 showed endogenous TRIM67 expression, whereas TS603 did not express TRIM67 (Supplementary Figure 2B). We transduced the SU-AO3s with shRNAs targeting TRIM67 to generate knockdown lines and ectopically expressed Flag-tagged TRIM67 in the other lines (Figure 1B, 2D). To gain insight into TRIM67 function, we performed RNA-seq on empty vector (EV) or TRIM67^{OE} TS603, S24, TS600, TS543, and hNPC cells and identified significantly altered genes upon TRIM67 overexpression (Supplementary Table 1). In the TS603 line, cytoskeleton/cell adhesion-associated genes accounted for the majority of differentially expressed genes (Supplementary Figure 2C). KEGG pathway and gene ontology analysis indicated the cytoskeleton and focal adhesion were among the most significantly altered pathways (Supplementary Figure. 2D). Pathways altered by TRIM67 in different cell lines revealed significant alteration of cytoskeleton-related pathways, such as paxillin signaling, Rho GTPase signaling, RAC signaling, integrin signaling and actin cytoskeleton signaling (Supplementary Figure 2E), suggesting a potentially ubiquitous role of TRIM67 in regulating cytoskeleton/cell adhesion-related pathways.

To further elucidate TRIM67-dependent mechanisms, we performed MS-based approaches using total cell extracts or TRIM67 pulldown using Flag antibody (Supplementary Table 2, Supplementary Figure 2F). The total cell extract-MS approach using 2 different ectopic TRIM67-expressing cell lines (TS603 and S24) showed a significant change in the abundance of cytoskeletal/cell adhesion proteins (Figure 1C–D, Supplementary Figure 2G), and the associated cytoskeletal, cell adhesion and Rho GTPase signaling pathways (Figure 1E–F). In the TRIM67-Flag coimmunoprecipitation (co-IP)-MS experiment in S24 cells, most TRIM67-interacting partners were cytoskeletal/cell adhesion proteins (Figure 1G, Supplementary Figure 2F). We compared

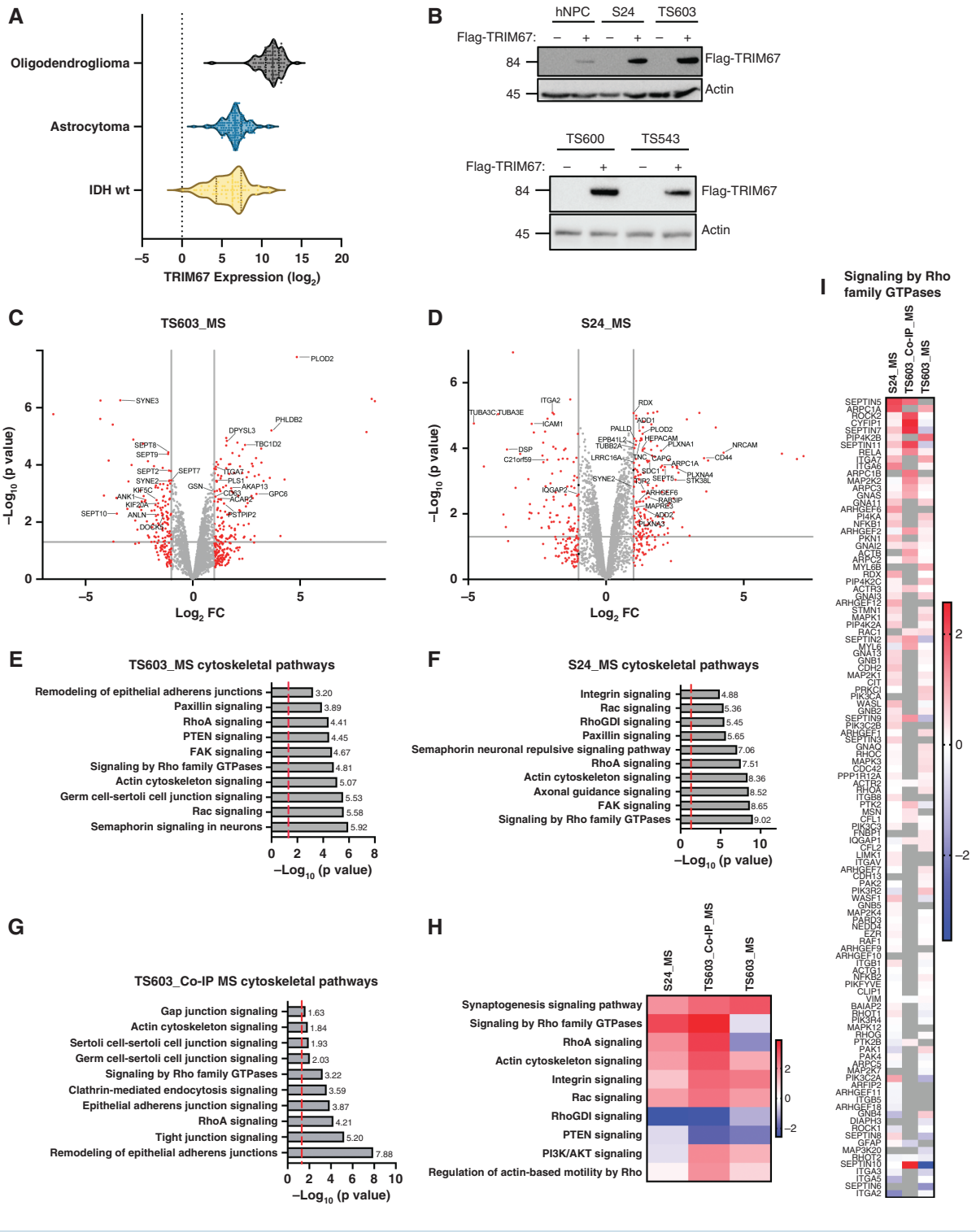

Figure 1. TRIM67 overexpression influences cytoskeletal proteins and pathways. **(A)** Bar plot shows $\log_2$ expression of *TRIM67* in oligodendrogliomas, astrocytomas, and IDH wild-type (wt) gliomas. The Cancer Genome Atlas LGG RNA-seq data were downloaded from GlioVis.[39] Histopathological classification is based on the 2007 WHO classification of CNS tumors. **(B)** Immunoblotting for Flag in EV (–) or TRIM67^{OE} (+) hNPC, S24, TS603 cells (upper panel) and TS600 and TS543 cells (lower panel). Actin serves as the loading control. **(C, D)** Volcano plots highlighting differentially abundant proteins shown in red ($-\log_{10}$[*P* value] >1,4, absolute[$\log_2$ fold change] > 1) identified by mass spectrometry (MS) in TRIM67^{OE} TS603 **(C)** or S24 cells **(D)** compared to EV control cells. Proteins of interest are shown in the plot. **(E-G)** Top 10 significantly enriched cytoskeletal pathways among the differentially abundant proteins ($-\log_{10}$[*P* value] >1,4) in TRIM67^{OE} TS603 (E), TRIM67^{OE} S24 (F), and Co-IP MS experiment in TRIM67^{OE} TS603 cells **(G)**. **(H)** Heatmap comparison of pathways enriched among the differentially abundant proteins in TRIM67^{OE} cells (S24_MS and TS603_MS) and the putative TRIM67 interacting partners in TS603 cells (TS603_Co-IP_MS). **(I)** Heatmap showing the differentially abundant signaling proteins within the Rho family GTPases for S24_MS, TS603_Co-IP_MS, and TS603_MS.

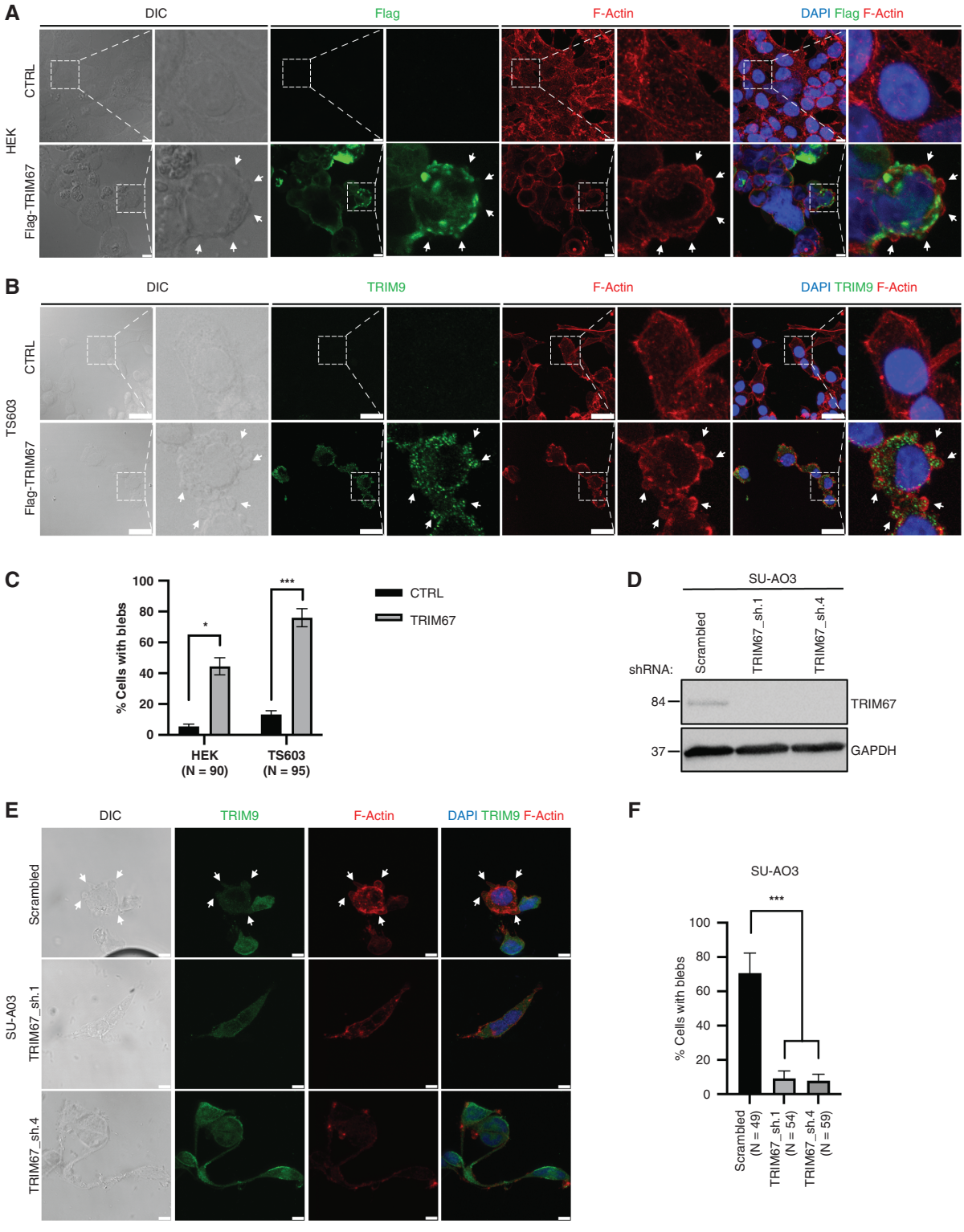

Figure 2. TRIM67 overexpression induces membrane blebbing and rounded cell morphology. **(A)** Representative IF images of EV or TRIM67^{OE} HEK293TN cells. DIC indicates bright-field images, Flag in green, F-Actin in red, and DAPI in blue. The zoomed regions of interest (ROI) are shown by white rectangles. Membrane blebs are indicated by white arrows. Scale bar, 10 μm. **(B)** Representative IF images of EV or TRIM67^{OE} TS603 cells. DIC indicates bright-field images, TRIM9 in green, F-Actin in red, and DAPI in blue. The zoomed ROI are shown by white rectangles. Membrane blebs are marked by white arrows. Scale bar, 25 μm. **(C)** Quantification of **(A)** and **(B)**. * $P < .05$, *** $P < .001$. **(D)** Immunoblotting for TRIM67 and GAPDH in SU-A03 cells transduced with scrambled shRNA, or TRIM67 shRNA (sh1 or sh4). **E)** Representative IF images of SU-A03 cells transduced with scrambled shRNA, TRIM67 shRNA (sh.1 or sh.4). DIC indicates bright-field images, TRIM9 in green, F-Actin in red, and DAPI in blue. Membrane blebs are indicated by white arrows. Scale bar, 8 μm. **(F)** Quantification of **(E)**. *** $P < .001$.

our independent MS experiments and analyzed the overlap of the differentially active pathways, which showed actin cytoskeleton and Rho GTPase signaling among the top hits (Figure 1H). Detailed examination of these pathways indicated several members of Rho family GTPases were altered (Figure 1I). Taken together, our high-throughput data suggest TRIM67 triggers changes in the cellular cytoskeleton, cell adhesion, and Rho GTPase signaling.

TRIM67 Influences the Structure or Expression of Cytoskeletal Proteins

Next, we aimed to address how TRIM67 affects cytoskeletal proteins. We performed immunofluorescence (IF) staining for a set of cytoskeletal proteins, including actin, tubulin, and F-actin. To observe the transient changes in the cytoskeletal structures upon TRIM67 ectopic expression, we transiently transfected HEK cells with actin-RFP or tubulin-RFP. IF showed actin-RFP and tubulin-RFP formed cytoskeletal clumps in HEK cells upon TRIM67 overexpression (Supplementary Figure 3A, C). F-actin levels decreased significantly upon TRIM67 overexpression in hNPCs and TS600s (Supplementary Figure 3B, D). F-actin levels were comparable in EV and TRIM67^{OE} TS603s but significantly reduced in TS600s by western blot (WB) (Supplementary Figure 3E–F). Of note, β-actin levels did not significantly alter upon TRIM67 overexpression (Supplementary Figure 3E–F). These results suggest that TRIM67 alters the abundance and distribution of cytoskeleton-associated proteins.

Ectopic TRIM67 Expression Induces the Formation of Membrane Blebs

We used confocal microscopy and F-actin staining to investigate how TRIM67 alters the cytoskeleton. In HEK cells, the morphology of epithelial-like adherent cells changed to a round cell structure upon transient TRIM67 transfection (Figure 2A). Remarkably, both differential interference contrast (DIC) and fluorescent F-actin images showed ectopic TRIM67 expression-induced membrane blebs, and TRIM67 clustered adjacent to the blebs (Figure 2A).

We next tested the interaction of TRIM67 with TRIM9, the TRIM family member with the closest sequence homology to TRIM67. Both proteins associate with the cytoskeleton,[7] regulate filopodia extension,[6] and play important roles in axon branching and synaptic vesicle formation.[8] Using WB, we detected a marked increase in TRIM9 levels in 3 glioma lines (Supplementary Figure 4A–B). We confirmed the physical interaction and coexistence of TRIM67 and TRIM9 by co-IP and IF (Supplementary Figure 4C–F). In HEK cells, transiently transfected TRIM9-GFP localized to cytoskeletal mesh-like fibers (Supplementary Figure 4E). Upon TRIM67 coexpression, this specific localization converted into a vesicle-like aggregate structure, in which TRIM67 and TRIM9 co-exist (Supplementary Figure 4E). The altered TRIM9 localization upon TRIM67 coexpression was confirmed with the Myc-TRIM9 construct (Supplementary Figure 4F), excluding a potential artifact caused by the GFP tag. Of note, TRIM67 and TRIM9 antibodies were specific and showed no cross-reactivity (Supplementary Figure 4G). Endogenous TRIM9 clustered with F-actin in the TRIM67-induced membrane blebs in the TS603 oligodendroglioma line (Figure 2B). The percentage of cells with membrane blebs increased several folds upon TRIM67 overexpression (Figure 2C).

Next, we validated the membrane blebbing phenotype with another patient-derived oligodendroglioma line, SU-AO3, with endogenous TRIM67 expression. To modulate TRIM67 levels, we performed overexpression or shRNA knockdown of TRIM67 (Supplementary Figure 5B, Figure 2D). SU-AO3s with scrambled shRNA exhibit membrane blebbing, and after TRIM67 knockdown, the bleb formation was inhibited and cells became more adherent (Figure 2E–F). Endogenous F-actin staining showed elongated F-actin morphology upon TRIM67 knockdown and partial colocalization with Flag-TRIM67 near membrane blebs (Supplementary Figure 5A, 5C). TRIM67-induced blebbing was more pronounced in TRIM67^{OE} than in control cells (Supplementary Figure 5D–E).

To further demonstrate the role of TRIM67 in membrane blebbing, we used the nonmuscle class II myosin inhibitor blebbistatin in TS603 cells. While blebbistatin had no significant effect on the F-actin structure and cytoskeleton morphology of control cells, TRIM67-induced membrane bleb formation was significantly inhibited and reverted to a more adherent phenotype with longer protrusions in TRIM67^{OE} cells after blebbistatin treatment (Supplementary Figure 6A–B). Overall, these data suggest ectopic TRIM67 expression triggers membrane blebbing and alters cytoskeletal proteins.

TRIM67-Driven Membrane Blebbing is Linked to Rho GTPase Signaling

We then investigated the mechanism by which TRIM67 triggers membrane blebbing. According to RNA-seq and MS data, Rho GTPases were highly altered upon TRIM67 overexpression (Supplementary Figure 2E and Figure 1E–I). Rho GTPase signaling plays a major role in cytoskeleton dynamics and membrane blebbing[20]; therefore, we hypothesized that TRIM67 may regulate Rho GTPase signaling to stimulate membrane blebbing. We performed GTP pulldown to detect the activity of GTP-bound Rho GTPases. This revealed significantly enhanced RHOA but reduced RAC1 activity in TRIM67^{OE} TS603 cells (Figure 3A–C). Consistently, RHOA-ROCK induces membrane blebbing whereas RAC1 suppresses it.[21] Indeed, we observed a significant increase in ROCK2 protein levels upon TRIM67 overexpression (Figure 3D–E).

To further test the involvement of ROCK signaling in TRIM67-driven blebbing, we used the selective ROCK inhibitor fasudil. F-actin cytoskeleton structure in control cells were not altered by fasudil treatment (Supplementary Figure 6C). However, inhibition of ROCK significantly reversed TRIM67-driven membrane blebbing (Figure 3H–I). To exclude the off-target effects of fasudil, we used other specific ROCK2 inhibitors, RKI-1447, and belumosudil. Both inhibitors decreased TRIM67-induced blebs (Supplementary Figure 8A–B). We next examined the Rho/ROCK upstream activator and neurite outgrowth inhibitor NOGO-A as a potential target

for TRIM67-induced blebbing.[22,23] Consistently, NOGO-A was upregulated in TRIM67-expressing cells by WB and IF (Figure 3F, G, J, L). Moreover, NOGO-A showed a similar distribution pattern and partial colocalization with F-actin and Flag-TRIM67 at specific sites (Figure 3J, K, M, N). These results suggest that TRIM67-induced membrane blebbing may result from altered NOGO-A/Rho GTPase/ROCK signaling.

To find ubiquitin-related targets of TRIM67, we performed a whole-cell extract-MS approach with or without the proteasomal inhibitor MG132 in TRIM67^{OE} TS603s. In MG132-treated cells, we detected an increased abundance of MYO6, an unconventional minus-end myosin involved in membrane ruffling by anchoring the plasma membrane to the cytoskeleton[24] as the top hit (Supplementary Figure 7A). We observed an interaction of TRIM67 with MYO6 after Flag-TRIM67 pulldown in S24 and TS603 cells (Supplementary Figure 7B, C). In addition, MYO6 localized in TRIM67-induced blebs partially overlapped with F-actin and Flag-TRIM67 (Supplementary Figure 7D–F). This suggests MYO6 could be targeted by TRIM67 and may play a role in regulating the blebbing phenotype.

TRIM67 Expression Promotes Cell Migration

Membrane blebbing can lead to increased cell migration or apoptosis.[25] To rule out apoptosis, we performed IF for apoptotic markers cleaved caspase-3 and cleaved PARP. Despite membrane blebbing, we did not detect apoptosis in TRIM67^{OE} TS600 and TS603 cells (Supplementary Figure 9A–B). To determine the effects of TRIM67 on cell migration and invasion, we performed WB to assess the expression of several migration/invasion markers. Levels of phospho-FAK, phospho-Akt, and vimentin increased, whereas tensin-2 was reduced upon TRIM67 overexpression (Figure 4A–B). Tensin-2 negatively regulates Akt signaling and consequently cell proliferation and migration,[26] suggesting that TRIM67 may activate cell migration and invasion pathways. To further test this hypothesis, we performed wound healing assays using a neuroblastoma cell line with endogenous TRIM67 expression (SK-N-BE(2)), a TRIM67-deficient TS600 line, and transiently transfected HEK cells. SK-N-BE(2) cells showed significantly reduced migration after TRIM67 knockdown (Figure 4C, Supplementary Figure 10A, B). Similarly, TS600s and HEKs had increased cell migration upon TRIM67 overexpression (Figure 4D, Supplementary Figure 10B–D). F-actin staining of the migratory cells in the wound healing assay showed natural TRIM67-expressing SK-N-BE(2) cells retained bleb-based cell migration, and membrane blebs were inhibited by TRIM67 knockdown (Figure 4E). On 5 distinct coating matrices, surface adhesion reduced significantly in TRIM67^{OE} TS603s (Figure 4F–G) and increased in SU-AO3s with TRIM67 knockdown (Supplementary Figure 8C–D). Treatment with fasudil or blebbistatin resulted in a partial yet significant reversal of TRIM67-driven reduced adhesion, linking Rho GTPase-dependent blebbing with tumorigenesis (Supplementary Figure 8E–F). These results indicate that TRIM67 leads to enhanced cell migration with poor cell adhesion, a hallmark of cancer.

TRIM67 Overexpression Leads to Increased Tumor Growth and Reduced Survival *In vivo*

To address whether TRIM67 is oncogenic *in vivo*, we orthotopically implanted EV or TRIM67^{OE} TS603s at 2 dilutions (5000 or 50 000 cells) into the frontal lobes of athymic nude mice. TRIM67 overexpression significantly increased tumor growth as measured by BLI, reaching significance on day 18 (50 000 cells) (Supplementary Figure 10F–H) or day 27 (5000 cells) post-implantation (Figure 5A, B). TRIM67 overexpression in TS603s resulted in a significantly reduced overall survival when 5000 cells per mouse were implanted (Figure 5C). The reduced survival was also recapitulated with 50 000 cells, albeit the difference in median overall survival was not as pronounced (Supplementary Figure 10I). Remarkably, implantation of SU-AO3 cells with TRIM67 knockdown led to a marked increase in overall survival (Figure 5D).

We performed H&E, Flag, and Ki-67 staining on 2 selected coronal sections from mice implanted with 50 000 EV or TRIM67^{OE} TS603s. Flag staining confirmed the sustained constitutive expression of TRIM67 *in vivo* and revealed a significantly higher tumor burden associated with TRIM67 overexpression as measured by H&E and deformation of brain anatomy (Figure 5E). Of note, we did not detect a significant difference in Ki-67 levels upon TRIM67 overexpression (Figure 5F) but H&E quantification showed a significantly higher tumor content when TRIM67 was overexpressed (Figure 5G). To investigate whether TRIM67-expressing cells are invasive *in vivo*, we performed immunohistochemistry with the EMT marker vimentin using a human-specific antibody to detect only the implanted tumor cells. Increased vimentin expression in cancer correlates well with increased tumor growth, invasion, and poor prognosis.[27] Region of interest analysis in randomly selected areas of the tumor margin showed a significant accumulation of vimentin in the cytoplasm surrounding the nucleus in TRIM67-overexpressing tumors (Figure 5H, I).

In conclusion, our study identified *TRIM67* as a novel oncogene in oligodendrogliomas. Mechanistically, our results show overexpressed TRIM67 alters Rho GT Pase signaling and induces membrane blebbing, triggering tumor migration and expansion with higher mortality.

Discussion

TRIM67 plays an essential role in neuronal development.[4,6–8] Here, we identify TRIM67 as an oncogene that may have major implications for oligodendroglioma pathology. Our results indicate that TRIM67 activates the NOGO-A/Rho GTPase/ROCK signaling-dependent membrane blebbing mechanism, leading to cell motility and tumor progression (Figure 5J).

TRIM67 plays a tumor-suppressive role in colon, gastric and lung cancers,[11,28,29] while functioning as an oncogene in NSCLC.[12] Our study shows oligodendroglioma is another example of a tumor in which TRIM67 functions as an oncogene, leading to reduced overall survival, increased tumor volume, and increased vimentin expression at the tumor margin in orthotopic oligodendroglioma implantation

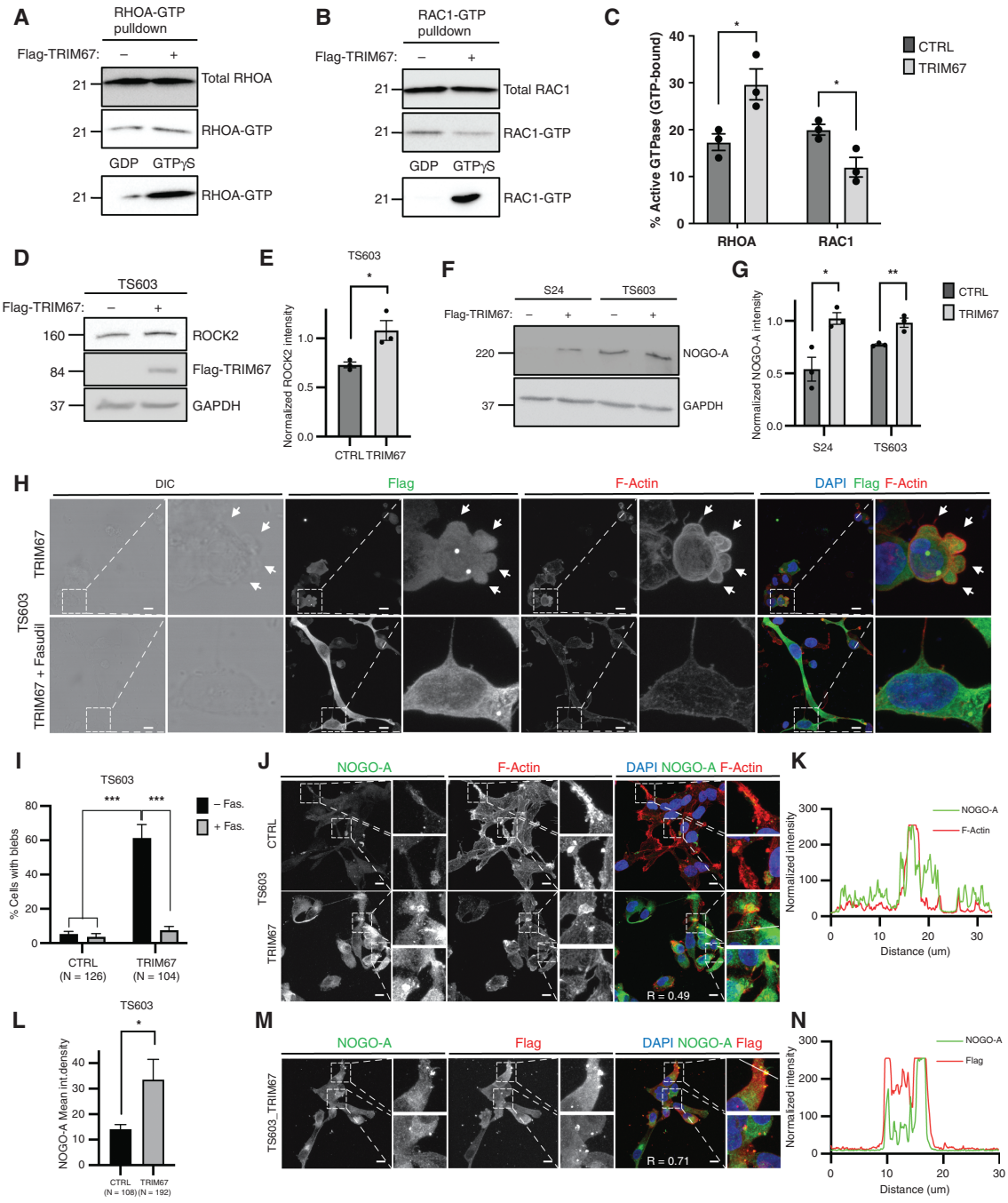

Figure 3. TRIM67 induces membrane blebbing through NOGO-A/Rho GTPase/ROCK signaling. **(A, B)** Immunoblotting for RHOA (A) or RAC1 **(B)** after GTP pulldown in EV or TRIM67^{OE} TS603 cells. GDP is used as a negative control and GTPγS as a positive control for GTP pulldown. **(C)** The normalized quantification for active RHOA and RAC1. Error bars indicate the standard error of the mean. Two-tailed t-test was performed, * $P < .05$. **(D)** Immunoblotting for Flag-TRIM67, ROCK2, and GAPDH in control and TRIM67^{OE} TS603 cells. GAPDH serves as a loading control. **(E)** Normalized quantification for ROCK2. **(F)** Immunoblotting for NOGO-A in EV and TRIM67^{OE} S24 and TS603 cells. GAPDH serves as the loading control. **(G)** Normalized quantification for NOGO-A is shown. **(H)** Representative IF images with and without fasudil treatment in TRIM67^{OE} TS603 cells. DIC indicates bright-field images, Flag in green, F-Actin in red, and DAPI in blue. The zoomed ROI are shown by white rectangles. Membrane blebs are marked by white arrows. Scale bar, 10 μm. **(I)** Bar plot indicates the percentage of cells with membrane blebbing with (+) or without (–) fasudil (Fas) treatment. **(J)** Representative IF images of control and TRIM67^{OE} TS603s. NOGO-A in green, F-Actin in red, and DAPI in blue. The zoomed ROI are shown by white rectangles. Scale bar, 8 μm. **(K)** Colocalization of NOGO-A and F-actin in the regions indicated by the white lines in (J) (3rd panel in the last column). **(L)** Bar plot showing the average intensity of NOGO-A in EV or TRIM67^{OE} TS603s. **(M)** Representative IF images of TRIM67^{OE} TS603 cells. NOGO-A in green, Flag in red, and DAPI in blue. The zoomed ROI are shown by white rectangles. Scale bar, 8 μm. **(N)** Colocalization of NOGO-A and Flag. A representative region for quantification is indicated by the white line in (M) (1st panel in the last column).

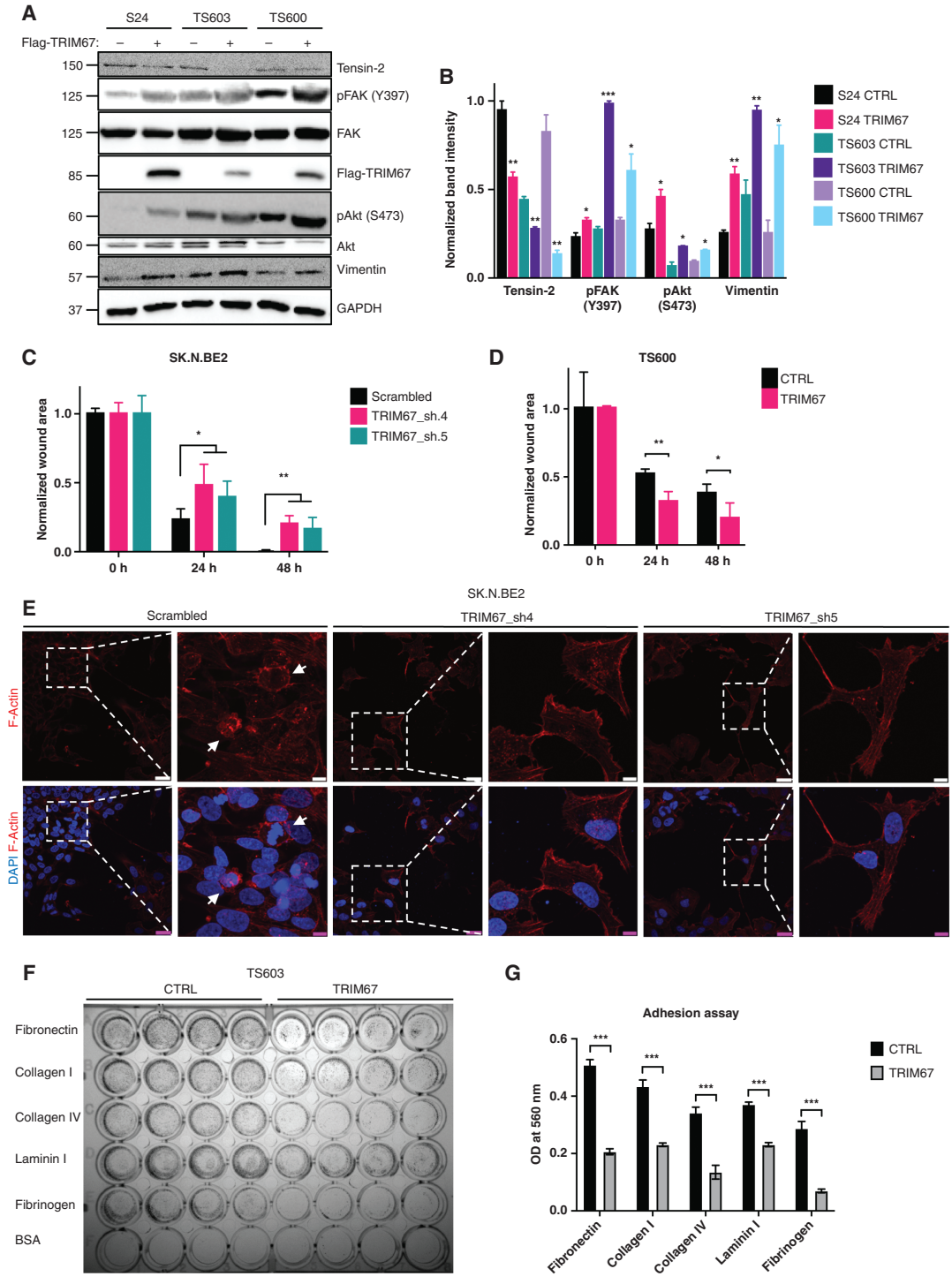

Figure 4. TRIM67 expression induces cell migration. **(A)** Immunoblotting for Tensin-2, pFAK, FAK, Flag-TRIM67, pAkt, Akt in EV (–) and TRIM67^{OE} (+) S24, TS603, and TS600 cells. GAPDH was used as the loading control. **(B)** The normalized quantification of **(A)**. pFAK and pAkt were also normalized to total FAK and Akt, respectively. Error bars indicate the standard error of the mean. Two-tailed t-test was performed, * $P < .05$, ** $P < .01$ and *** $P < .001$. **(C, D)** The quantification of Supplementary Figure 10B for normalized wound area in SK.N.BE2 cells transduced with scrambled shRNA or TRIM67 shRNA (sh4 and sh5) **(C)** and control or TRIM67^{OE} TS600 cells **(D)**. Error bars indicate the standard error of the mean. Two-tailed t-test was performed, * $P < .05$ and ** $p < .01$. **(E)** Representative IF images of wound healing in SK.N.BE2 cells transduced with scrambled shRNA or TRIM67 shRNA (sh4 and sh5). F-Actin in red and DAPI in blue. Bleb-based migrating cells are marked by white arrows. Scale bar, 10 μm. **(F)** Cell adhesion assay showing control and TRIM67^{OE} TS603 cells on 5 different coating matrices. BSA (bovine serum albumin) serves as the negative control. **(G)** Quantification of **(F)**. Error bars indicate the standard error of the mean. Two-tailed t-test was performed, *** $P < .001$.

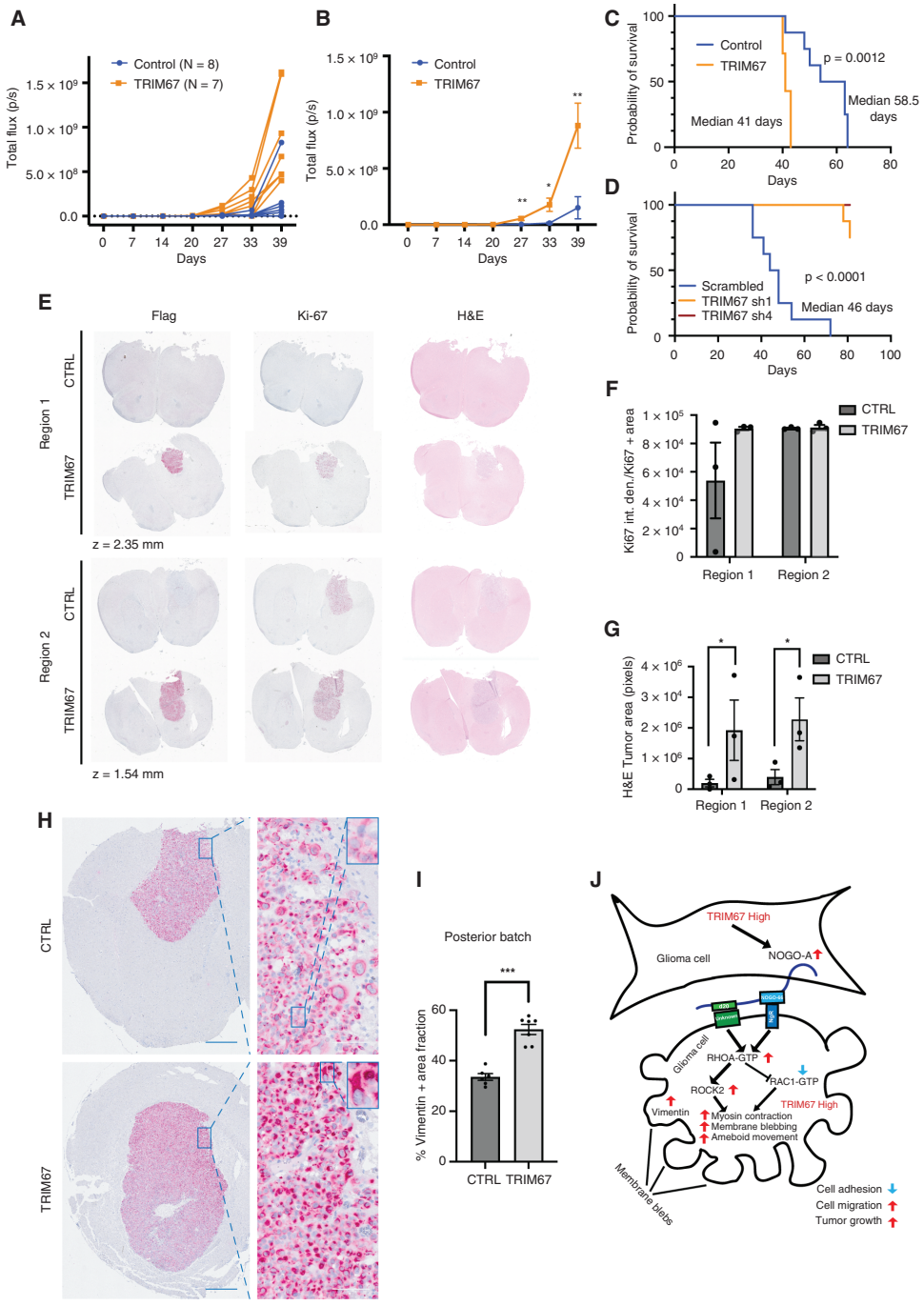

Figure 5. TRIM67 acts as an oncogene in oligodendroglioma implantation models. **(A)** Serial BLI imaging after implantation of control or TRIM67^{OE} TS603s (5000 cells injected) was shown for individual mice. **(B)** Average signal for BLI in **(A)**. Two-tailed t-test was performed, * $P < .05$, ** $P < .01$. **(C)** Kaplan-Meier survival curve of EV and TRIM67^{OE} TS603s (5000 cells injected). Log-rank test was performed, $P = .0012$. **(D)** Kaplan-Meier survival curve of SU-A03 transduced with scrambled or TRIM67 shRNAs (sh1, sh4). Log-rank test was performed, $P < .0001$. **E)** IHC images for Flag, Ki-67, and H&E using brain sections at 2 different regions from representative mice implanted with control or TRIM67^{OE} TS603s (50 000 cells injected). **(F, G)** Quantification of Ki-67 (F) and H&E (G). **(H)** Representative images of vimentin IHC in 5 μm thick coronal sections of mouse brains implanted with control or TRIM67^{OE} TS603s (50 000 cells injected) (left); scale bar, 1 cm. Zoomed-in regions around the tumor edge showing vimentin IHC (red); scale bar, 875 μm. **(I)** ROI (3 areas per section) quantification of vimentin within the tumor edge. Representative offset (blue window) is shown in H (right panel) (control = 16 sections, TRIM67 = 36 sections, two-tailed t-test was performed) *** $P < .001$. Error bars indicate the standard error of the mean. **(J)** Model illustrating the TRIM67-induced membrane blebbing in gliomas. Upregulated TRIM67 induces NOGO-A, which activates RHOA/ROCK2 signaling but inhibits RAC1 signaling. TRIM67 expression leads to actomyosin contractility and membrane blebbing, in turn reducing cell adhesion, increasing cell migration, vimentin expression at the tumor margin, and tumor growth.

models. Although further studies are needed, our findings suggest an oncogenic role for TRIM67 in neuroblastoma. Overall, the broad spectrum of mechanistic and phenotypic roles of TRIM67 in various cancers suggests its function is highly tissue-dependent. An interesting point to be explored in future studies may be to determine the similar features between oligodendrogliomas and NSCLC that permit the oncogenic functions of TRIM67 to emerge.

Remarkably, a large number of TRIM proteins play an oncogenic role in gliomas,[30-34] with TRIM3 being an exception.[35] In this context, TRIM67 emerges as another member of the TRIM family with an oncogenic function in gliomas. The TRIM-protein family has E3 ubiquitin ligase activity, and direct ubiquitination targets of TRIM67 have been restricted to 80-K-H, such that TRIM67-induced degradation of 80-K-H leads to altered Ras signaling.[10] In a recent MS-based study,[7] potential TRIM67 and TRIM9 ubiquitination targets were discovered in primary mouse cortical neurons, with NOGO-A as a potential ubiquitination target of TRIM67 that requires further functional characterization in the context of gliomas. Our MS experiments with patient-derived glioma tumorspheres provide candidates, including MYO6, to investigate potential TRIM67 targets. Comparison of TRIM67 interactome between primary gliomas and mouse cortical neurons may lead to the discovery of key TRIM67 targets underlying tumorigenesis.

Crosstalk between TRIM9 and TRIM67 also needs further investigation. It has been suggested that TRIM9 and TRIM67 may act antagonistically by regulating VASP degradation and filopodia extension.[6] However, ubiquitylome analysis in mouse cortical neurons indicated TRIM9 and TRIM67 could have redundant and nonredundant functions.[7] Our study shows enrichment of TRIM9 protein levels upon TRIM67 overexpression, and physical interaction and colocalization of TRIM9 with TRIM67. However, further efforts are needed to fully elucidate the TRIM67/TRIM9 interaction axis and crosstalk with other TRIMs in gliomagenesis.

Recent efforts have focused on mapping the TRIM67 interactome. Using the Bio-ID-MS approach, Menon *et al.* reported the interacting partners of TRIM67 mainly consist of cytoskeletal, synaptic, exocytosis, and endocytosis proteins in mouse cortical neurons.[7] Similarly, our IP-MS and total lysate-MS data demonstrate that the TRIM67 interactome contains mainly proteins associated with the cytoskeleton, endocytosis, cell adhesion, and cell junction. Moreover, our work identifies additional TRIM67-targeted pathways, such as Rho GTPase, RhoA, and Rac signaling. These altered signaling pathways may underlie glioma pathogenesis. For example, metastatic cancer cells benefit from both elongated and rounded modes of migration.[36] These two different modes of movement are regulated by Rho GTPases. Elongated cell migration is driven by RAC1 activity and couples with F-actin-containing protrusions and extracellular matrix (ECM) degradation. On the other hand, bleb-based rounded cell migration is triggered by RHOA/C signaling-mediated ROCK activity and accompanied by actomyosin contractility without the need for ECM proteolysis.[37] Bleb-based rounded cell motility predominates when active Rho-ROCK signaling is coupled with suppressed RAC1 signaling.[21] Consistently, our results indicate activated Rho-ROCK and inhibited RAC1 signaling may underlie the TRIM67-driven membrane blebbing. Active RHOA signaling is expected to increase levels of cytoskeletal proteins, including F-actin. We detect enrichment of some cytoskeletal proteins, but we identify a significant reduction in F-actin levels in TRIM67^{OE} hNPCs and TS600s. One reason may be that TRIM67-induced filopodia dynamics, exocytosis, and synaptic vesicle formation lead to the loss of cell membrane and cytoskeleton structures, resulting in reduced phalloidin staining.

From a translational perspective, a comprehensive evaluation of the transcriptional changes that distinguish oligodendrogliomas from astrocytomas could ultimately serve either as a therapeutic target or as a pathological biomarker to distinguish subtypes when additional markers are needed. Indeed, TRIM67 has recently been shown to be a highly abundant protein that distinguishes oligodendrogliomas.[38] Our work has revealed a functional pathogenic mechanism and points to a basis for a new therapeutic strategy. Inhibition of the Rho-ROCK pathway may be considered an additional or complementary therapeutic option for oligodendrogliomas. In addition, targeting bleb-based cell motility could be an alternative strategy. Such therapeutic options could be explored in combination with other therapies currently being tested in clinical trials for IDH mutant gliomas, including IDH inhibitors. In conclusion, our results highlight TRIM67 as a highly expressed gene in oligodendrogliomas, point to the inhibition of TRIM67-mediated pathways as a viable therapeutic target, and demonstrate the potential use of TRIM67 as a biomarker unique to oligodendrogliomas.

Supplementary Material

Supplementary material is available online at *Neuro-Oncology* (http://neuro-oncology.oxfordjournals.org/).

Keywords

E3 ligase | Rho GTPase signaling | glioma | membrane blebbing | mouse | TRIM67

Acknowledgments

We thank Turcan lab members for their helpful discussions. We thank the Genomics and Proteomics Core Facility (GPCF) of DKFZ for next-generation sequencing (NGS) and proteomics services and analysis. We thank the Omics IT and Data Management Core Facility (ODCF) of DKFZ for data management and technical support.

Funding

This work was supported by the German Cancer Aid, Max Eder Program grant number 70111964 (S.T.) and DFG Project-ID 404521405, SFB 1389 – UNITE Glioblastoma, Work package A04 (S.T.). J.T. is supported by a DFG Mercator Fellowship (DFG grant number TU 585/1-1).

Conflict of Interest: The authors declare no conflicts of interest.

Authorship

E.D. and S.T. designed and directed the study. R. A. identified TRIM67 upregulation from bioinformatic analyses. E.D., R.A., A.N., X.S., J.P.V., and B.S. performed the experiments. E.D., R.A., A.N., and S.T. analyzed the data. E.D., A.N., J.T., and S.T interpreted the data. M.B., D.K., C.S., and G.S. provided technical assistance. D.K. provided custom-built macro plugins for image analysis. F.B. and J.T. provided conceptual advice. E.D. and S.T. wrote the paper. All authors contributed to the writing and/or editing of the manuscript.

References

1. Brat DJ, Verhaak RG, Aldape KD, et al. Comprehensive, integrative genomic analysis of diffuse lower-grade gliomas. *N Engl J Med.* 2015; 372(26):2481–2498.
2. Yan H, Parsons DW, Jin G, et al. IDH1 and IDH2 mutations in gliomas. *N Engl J Med.* 2009;360(8):765–773.
3. Hatakeyama S. TRIM family proteins: roles in autophagy, immunity, and carcinogenesis. *Trends Biochem Sci.* 2017;42(4):297–311.
4. Boyer NP, Monkiewicz C, Menon S, Moy SS, Gupton SL. Mammalian TRIM67 functions in brain development and behavior. *eNeuro.* 2018;5(3):ENEURO.0186–ENEU18.2018.
5. Montell DJ. TRIMing neural connections with ubiquitin. *Dev Cell.* 2019;48(1):5–6.
6. Boyer NP, McCormick LE, Menon S, Urbina FL, Gupton SL. A pair of E3 ubiquitin ligases compete to regulate filopodial dynamics and axon guidance. *J Cell Biol.* 2020;219(1):e201902088.
7. Menon S, Goldfarb D, Ho CT, et al. The TRIM9/TRIM67 neuronal interactome reveals novel activators of morphogenesis. *Mol Biol Cell.* 2021;32(4):314–330.
8. Urbina FL, Menon S, Goldfarb D, et al. TRIM67 regulates exocytic mode and neuronal morphogenesis via SNAP47. *Cell Rep.* 2021;34(6):108743.
9. Do LD, Gupton SL, Tanji K, et al. TRIM9 and TRIM67 are new targets in paraneoplastic cerebellar degeneration. *Cerebellum.* 2019;18(2):245–254.
10. Yaguchi H, Okumura F, Takahashi H, et al. TRIM67 protein negatively regulates Ras activity through degradation of 80K-H and induces neuritogenesis. *J Biol Chem.* 2012;287(15):12050–12059.
11. Wang S, Zhang Y, Huang J, et al. TRIM67 activates p53 to suppress colorectal cancer initiation and progression. *Cancer Res.* 2019;79(16):4086–4098.
12. Jiang J, Ren H, Xu Y, et al. TRIM67 promotes the proliferation, migration, and invasion of non-small-cell lung cancer by positively regulating the notch pathway. *J Cancer* 2020;11(5):1240–1249.
13. Schönrock A, Heinzelmann E, Steffl B, et al. MEOX2 homeobox gene promotes growth of malignant gliomas. *Neuro Oncol.* 2022;24(11):1911–1924.
14. Schindelin J, Arganda-Carreras I, Frise E, et al. Fiji: an open-source platform for biological-image analysis. *Nat Methods.* 2012;9(7):676–682.
15. Love MI, Huber W, Anders S. Moderated estimation of fold change and dispersion for RNA-seq data with DESeq2. *Genome Biol.* 2014;15(12):550.
16. Afgan E, Baker D, Batut B, et al. The Galaxy platform for accessible, reproducible and collaborative biomedical analyses: 2018 update. *Nucleic Acids Res.* 2018;46(W1):W537–W544.
17. Kuleshov MV, Jones MR, Rouillard AD, et al. Enrichr: a comprehensive gene set enrichment analysis web server 2016 update. *Nucleic Acids Res.* 2016;44(W1):W90–W97.
18. Corces MR, Granja JM, Shams S, et al. The chromatin accessibility landscape of primary human cancers. *Science.* 2018;362(6413):eaav1898.
19. Al-Ali R, Bauer K, Park JW, et al. Single-nucleus chromatin accessibility reveals intratumoral epigenetic heterogeneity in IDH1 mutant gliomas. *Acta Neuropathol Commun* 2019;7(1):201.
20. Clayton NS, Ridley AJ. Targeting Rho GTPase signaling networks in cancer. *Front Cell Dev Biol.* 2020;8:222.
21. Sanz-Moreno V, Gadea G, Ahn J, et al. Rac activation and inactivation control plasticity of tumor cell movement. *Cell.* 2008;135(3):510–523.
22. Fujita Y, Yamashita T. Axon growth inhibition by RhoA/ROCK in the central nervous system. *Front Neurosci.* 2014;8:338.
23. Schwab ME. Functions of Nogo proteins and their receptors in the nervous system. *Nat Rev Neurosci.* 2010;11(12):799–811.
24. Chibalina MV, Poliakov A, Kendrick-Jones J, Buss F. Myosin VI and optineurin are required for polarized EGFR delivery and directed migration. *Traffic.* 2010;11(10):1290–1303.
25. Fackler OT, Grosse R. Cell motility through plasma membrane blebbing. *J Cell Biol.* 2008;181(6):879–884.
26. Hafizi S, Ibraimi F, Dahlback B. C1-TEN is a negative regulator of the Akt/PKB signal transduction pathway and inhibits cell survival, proliferation, and migration. *FASEB J.* 2005;19(8):971–973.
27. Satelli A, Li S. Vimentin in cancer and its potential as a molecular target for cancer therapy. *Cell Mol Life Sci.* 2011;68(18):3033–3046.
28. Liu Y, Wang G, Jiang X, et al. TRIM67 inhibits tumor proliferation and metastasis by mediating MAPK11 in Colorectal Cancer. *J Cancer* 2020;11(20):6025–6037.
29. Liu R, Chen Y, Shou T, et al. TRIM67 promotes NFkappaB pathway and cell apoptosis in GA13315treated lung cancer cells. *Mol Med Rep.* 2019;20(3):2936–2944.
30. Feng S, Cai X, Li Y, et al. Tripartite motif-containing 14 (TRIM14) promotes epithelial-mesenchymal transition via ZEB2 in glioblastoma cells. *J Exp Clin Cancer Res.* 2019;38(1):57.
31. Ji J, Ding K, Luo T, et al. TRIM22 activates NF-kappaB signaling in glioblastoma by accelerating the degradation of IkappaBalpha. *Cell Death Differ.* 2021;28(1):367–381.
32. Qi ZX, Cai JJ, Chen LC, et al. TRIM28 as an independent prognostic marker plays critical roles in glioma progression. *J Neurooncol.* 2016;126(1):19–26.
33. Shi G, Lv C, Yang Z, et al. TRIM31 promotes proliferation, invasion and migration of glioma cells through Akt signaling pathway. *Neoplasma.* 2019;66(5):727–735.
34. Tang SL, Gao YL, Wen-Zhong H. Knockdown of TRIM37 suppresses the proliferation, migration and invasion of glioma cells through the inactivation of PI3K/Akt signaling pathway. *Biomed Pharmacother.* 2018;99:59–64.
35. Liu Y, Raheja R, Yeh N, et al. TRIM3, a tumor suppressor linked to regulation of p21(Waf1/Cip1.). *Oncogene.* 2014;33(3):308–315.
36. Yamada KM, Sixt M. Mechanisms of 3D cell migration. *Nat Rev Mol Cell Biol.* 2019;20(12):738–752.
37. Wyckoff JB, Pinner SE, Gschmeissner S, Condeelis JS, Sahai E. ROCK- and myosin-dependent matrix deformation enables protease-independent tumor-cell invasion in vivo. *Curr Biol.* 2006;16(15):1515–1523.
38. Felix M, Friedel D, Jayavelu AK, et al. HIP1R and Vimentin immunohistochemistry predict 1p/19q status in IDH-mutant glioma. *Neuro Oncol.* 2022;24(12):2121–2132.
39. Bowman RL, Wang Q, Carro A, Verhaak RG, Squatrito M. GlioVis data portal for visualization and analysis of brain tumor expression datasets. *Neuro Oncol.* 2017;19(1):139–141.